科学通报

Near-field optical characterization of low-dimensional nanomaterials

胡德波 and 戴庆

Citation: 科学通报 **63**, 3747 (2018); doi: 10.1360/N972018-00864

View online: http://engine.scichina.com/doi/10.1360/N972018-00864

View Table of Contents: http://engine.scichina.com/publisher/scp/journal/CSB/63/35

Published by the 《中国科学》杂志社

科学通报 2018 年 第 63 卷 第 35 期: 3747 ~ 3759
专辑: 庆祝国家纳米科学中心成立15周年 评 述
《中国科学》杂志社
SCIENCE CHINA PRESS

低维纳米材料的近场光学表征

胡德波, 戴庆*

国家纳米科学中心纳米光子学研究部, 北京 100190
* 联系人, E-mail: daiq@nanoctr.cn

2018-08-21 收稿, 2018-09-18 修回, 2018-09-21 接受, 2018-10-25 网络版发表
国家重大科学研究计划(2015CB932400)、国家自然科学基金(11704085)和中国科学院仪器研制项目资助

摘要 光学显微术作为一种快速、无损的表征手段在材料研究领域得到了广泛应用, 但是受光的波动性制约, 传统远场光学显微术无法满足低维纳米材料表征对亚衍射极限空间分辨率的需求. 近年来, 随着散射式扫描近场光学显微术(s-SNOM)的发展进步, 光学成像的空间分辨率已经达到10 nm量级, 突破了光学衍射极限. 本文首先简要阐述了s-SNOM的成像原理, 然后按照s-SNOM的工作模式分类介绍了其在低维纳米材料表征领域的应用研究进展, 最后对s-SNOM技术未来的发展及应用进行展望.

关键词 衍射极限, 低维材料, 近场成像, 电磁模式, 纳米红外

光学显微术是材料研究领域应用广泛、结果直观的重要表征技术. 然而, 光的波动性决定了传统光学显微术的空间分辨率存在一个固有的极限——衍射极限. 对于一个衍射受限光学系统, 其空间分辨率仅由工作波长和数值孔径决定, 约为半波长量级[1]; 在可见光波段, 这一极限对应于200~300 nm的空间分辨率; 而在红外波段, 这一极限则对应微米量级的空间分辨率, 远大于纳米材料的典型尺寸1~100 nm[2]. 为了满足纳米材料研究对亚衍射极限空间分辨率的迫切需求, 多种突破衍射极限的新型光学显微成像技术应运而生, 如受激发射损耗显微术(stimulated emission depletion microscopy, STED)[3], 光激活定位显微术(photoactivated localization microscopy, PALM)[4], 随机光学重构显微术(stochastic optical reconstruction microscopy, STORM)[5], 以及扫描近场光学显微术(scanning near-field optical microscopy, SNOM)[6]等. 其中, 前3种都是对传统远场光学显微术的改进[7], 分别利用结构光照明和单荧光分子定位来实现超分辨成像. 因为事先需要利用荧光染料或荧光蛋白对样品进行标记, 较适合于生物材料的表征. SNOM利用光学近场实现超分辨成像, 是扫描隧道显微术(scanning tunneling microscopy, STM)[8]在光学中的对应技术, 无需对样品进行任何标记, 较适合于非生物纳米材料的光学表征. 此外, 针尖增强拉曼光谱技术(tip-enhanced Raman scattering, TERS)作为传统光谱技术与近场光学技术的有机结合, 在超分辨成像领域也取得了显著进展[9].

光照射物体发生散射时, 散射场以两种形式存在: 辐射场和倏逝场[10]. 其中, 辐射场可以在空间自由传播到达远离散射体的区域, 因而又被称为远场; 倏逝场总是附着于散射体表面, 其强度随与表面距离的增大迅速衰减, 不能到达远离散射体的区域, 因而又被称为近场. 近场信息的缺失是传统远场光学显微术空间分辨率受限的根本原因[11]. 为实现超分辨光学成像, 散射体的近场光学信息必须得到有效利用[12]. 实际上, 在人们对近场光学有所了解之前已经有多位学者先后提出了利用亚波长尺寸的通光孔径或金属粒子抵近散射体表面进行扫描从而实现

引用格式: 胡德波, 戴庆. 低维纳米材料的近场光学表征. 科学通报, 2018, 63: 3747–3759
Hu D B, Dai Q. Near-field optical characterization of low-dimensional nanomaterials (in Chinese). Chin Sci Bull, 2018, 63: 3747–3759, doi: 10.1360/N972018-00864

超分辨光学成像的思想[13~15]. 由于当时的技术条件不能满足以纳米级精度控制物体间距并实现横向扫描的要求, 这一思想只能停留在纸面上. 直到20世纪80年代, 随着扫描探针技术的兴起, SNOM的实现才成为可能[16,17].

早期的SNOM仪器多使用孔径式近场探针[18~20], 因此被称为孔径式扫描近场光学显微镜(apertured SNOM, a-SNOM); 随后又发展出了利用散射式探针获取近场信号的散射型扫描近场光学显微镜(scattering-type SNOM, s-SNOM)[21~24]. 由于孔径式和散射式近场探针周围的电磁场分别类似于磁偶极子和电偶极子的场, a-SNOM和s-SNOM在偏振分辨近场成像方面具有一定的互补性[25~27]. a-SNOM一般利用光纤将激发光导向孔径或将近场信号馈入探测器, 因而其遭受的背景干扰小, 不需要采取复杂的背景抑制措施; 但是由于光纤和孔径均存在截止现象(传输波长存在上限), a-SNOM的工作频段较窄并且其空间分辨率依赖于工作波长[28], 尤其是在中红外及太赫兹频段a-SNOM的空间分辨能力快速衰减[29]. 与之相反, s-SNOM通过自由空间将激发光导向探针或将近场信号收集进入探测器, 工作频段较宽并且其空间分辨率仅由探针尖端的曲率半径决定而与工作波长无关[30]; 虽然上述空间照明方式会引入大量背景干扰, s-SNOM通过采用适当的调制-解调方法可以显著地抑制干扰, 实现高信噪比的近场光学成像[31].

由于上述性能方面的显著优势, 近年来s-SNOM技术的发展推动了低维纳米材料近场光学表征领域的快速发展[32]. 本文将首先介绍s-SNOM的工作原理, 然后分类介绍其在低维纳米材料表征领域的应用研究进展, 最后对全文进行总结, 并对s-SNOM技术未来的发展方向进行展望.

1 s-SNOM工作原理

如图1(a)所示, s-SNOM主要由光学系统及原子力显微系统(AFM)两大部分组成. 其中光学系统由一套非对称迈克尔逊干涉仪构成, AFM探针和一面反射镜分别位于干涉仪两臂的端点. 该光学系统的主要功能有2个: (1) 将激发光导入AFM并聚焦到近场探针尖端; (2) 收集近场探针的散射信号并利用其与参考光(由反射镜返回)的干涉提高信号的信噪比. AFM负责逐点扫描样品并将探测器的输出拼合成二维图像. 近场探针是s-SNOM最关键的元件, 其在激发光照射下与样品之间的相互作用是s-SNOM成像对比度的来源. 而要提取真实的近场信号以获得高质量的近场图像, 合适的调制-解调方法必不可少.

1.1 成像对比度来源

在图1(a)中, 激发光聚焦后的光斑大小在微米量级, 近场探针的尺寸一般为几十到上百微米, 而探针能够与样品进行有效相互作用的尖端部分尺寸仅有一二十纳米, 因此激发光-近场探针-样品三者之间的相互作用是一个跨越多个尺度的复杂电磁问题, 一般不存在闭式解. 不过仍然可以通过适当简化的物理模型来定性或半定量地理解s-SNOM成像对比度的来源.

s-SNOM中的金属近场探针可以被看作光学天线[33,34]. 首先, 探针在聚焦光束的照射下在其尖端附近诱导出强电磁场并对激发光产生弹性散射[35]; 其次, 当探针和样品相互靠近进入光学近场的作用范围时, 样品会改变探针尖端的电磁场, 探针-样品作为一个整体对激发光的弹性散射由此携带了样品的

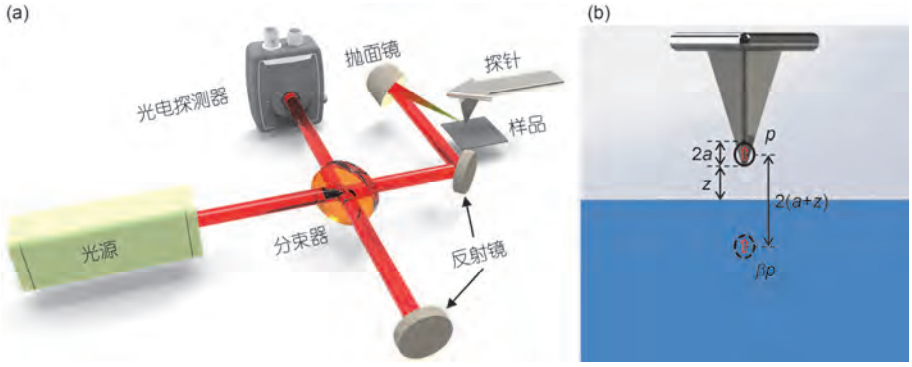

图 1 s-SNOM工作原理. (a) s-SNOM结构图; (b) 近场探针与样品相互作用的偶极模型

Figure 1 Working principles of s-SNOM. (a) Schematic diagram of s-SNOM. (b) Dipole model for the tip-sample interaction

光学性质信息. 在对样品进行逐点扫描时, 如果样品在不同位置的光学性质有差异, 探测器接收到的弹性散射光的特征(振幅, 相位等)也会随之改变, 这就是s-SNOM成像对比度的来源.

考虑到真正与样品发生较强相互作用的仅仅是探针的尖端部分, 可以忽略探针其余部分的影响将其简化为一个球体, 进而得到一个描述探针-样品相互作用的半定量模型——偶极模型[36,37], 如图1(b)所示. 该等效球体的半径为探针尖端的曲率半径a, 若探针材料的相对介电常数为$\varepsilon_{\rm t}$, 则当a远小于激发光波长λ时, 整个球体的极化率为[38]

$$\alpha_{\rm t}=4\pi a^3\frac{\varepsilon_{\rm t}-\varepsilon_{\rm a}}{\varepsilon_{\rm t}+2\varepsilon_{\rm a}}, \tag{1}$$

其中, $\varepsilon_{\rm a}$为探针周围环境的相对介电常数, 一般可取为1. 当探针和样品相互靠近时, 探针的偶极矩p可在样品内部感生出一个方向相同大小为βp的镜像偶极矩, 其中β是样品表面的静态反射系数, 可用样品的相对介电常数$\varepsilon_{\rm s}$表示为[39]

$$\beta=\frac{\varepsilon_{\rm s}-\varepsilon_{\rm a}}{\varepsilon_{\rm s}+\varepsilon_{\rm a}}. \tag{2}$$

随后, 探针偶极和样品偶极之间通过它们在对方附近产生的电场互相增强. 最终, 探针-样品整个系统的极化率可表示为这一系列相互作用的叠加[36,40]:

$$\alpha_{\rm ts}=\frac{\alpha_{\rm t}(1+\beta)}{1-\dfrac{\alpha_{\rm t}\beta}{16\pi(a+z)^3}}, \tag{3}$$

其中, z为探针尖端与样品表面的距离. 这样, 当探针尖端附近的激发光电场为$E_{\rm i}$时, s-SNOM探测器可接收到的近场散射信号为$E_{\rm ts}\propto a_{\rm ts}\varepsilon_0 E_{\rm i}$, 其中$\varepsilon_0$为真空介电常数. 以通讯波段$\lambda$=1.5 μm处的铂探针($\varepsilon_{\rm t}$=−252+55$i$)及硅样品($\varepsilon_{\rm s}$=12)为例, 由式(3)计算可得近场散射信号的振幅及相位(取a=10 nm, 振幅指散射光与激发光场强之比, 相位指散射光与激发光相位之差), 如图2(a), (b)所示. 可见近场信号对探针-样品之间的距离有很强的依赖关系.

需要注意的是, 在上述偶极模型的建立过程中我们并未对探针的材料进行限定. 虽然在s-SNOM实验中金属探针的应用最为广泛, 由其他材料——尤其是高折射率介电材料构筑的探针同样不可或缺, 例如硅探针. 在特定的应用场景中, 非金属探针的性能会优于

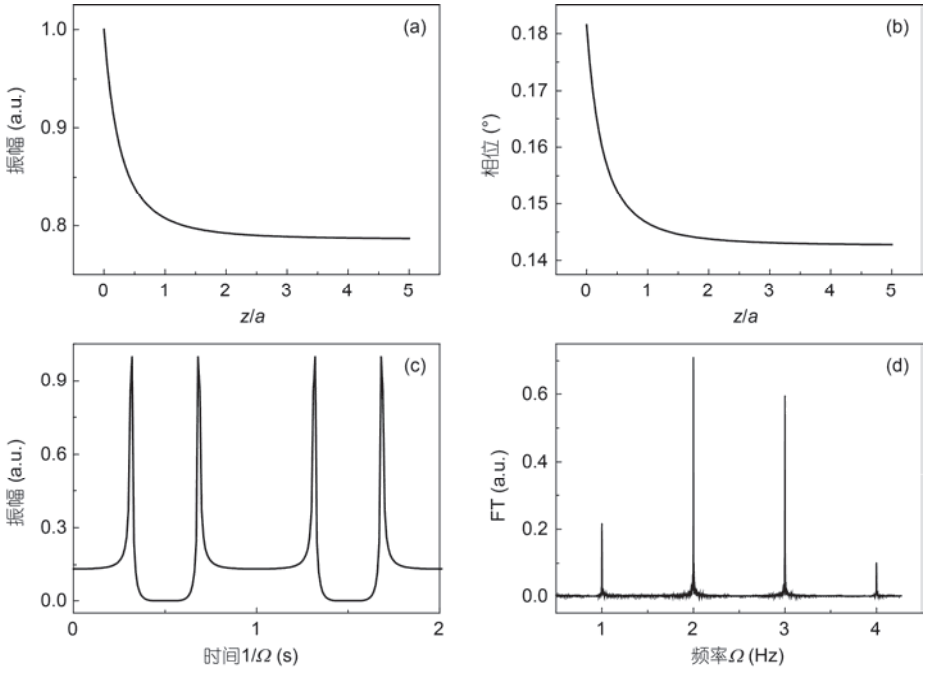

图 2 近场信号调制-解调原理. (a), (b) 近场信号振幅及相位与探针-样品距离z的关系; (c) 以频率Ω及振幅a对z进行正弦调制时近场信号振幅随时间的变化; (d) 对(c)进行傅里叶变换得到近场信号在探针调制频率Ω各阶泛频的分量

Figure 2 Modulation-demodulation principles of near-field signals. (a), (b) Nonlinear dependences of near-field amplitude and phase on the tip-sample distance z. (c) Temporal variation of the near-field amplitude corresponding to the modulation frequency Ω and modulation depth a. (d) Components of the near-field signal at different harmonics of the tip tapping frequency can be obtained by imposing Fourier transform on the curve in (c)

金属探针, 具体事例我们将在下文相关部分阐述.

1.2 调制-解调原理

由于探针和样品发生有效相互作用的体积远小于激发光光斑的大小, 近场散射信号往往被很强的背景散射淹没[41]. 要从大量背景噪声中提取出真实的近场信号, 必须对其进行标记, 即信号调制. 由图2(a)可知, 近场信号的振幅对探针-样品间距z有很强的非线性依赖; 而背景噪声一般来源于探针非尖端部分及样品表面对激发光的直接散射, 对z有接近线性的依赖关系[42]. 因而可以通过对z进行正弦调制实现对近场信号的标记[43], 在探测器端通过提取探针调制频率Ω各高阶泛频的分量进行信号解调[44,45]. 图2(c)模拟了以10 nm振幅对z进行调制时近场信号振幅随时间的变化过程, 非线性效应使得曲线偏离了规则的正弦振荡, 包含了大量高频信息; 对图2(c)进行傅里叶变换(Fourier transform, FT)可得到其频谱, 如图2(d)所示, 从中可以得到各阶近场信号的强度. 在真实的s-SNOM仪器中, Ω一般为几十到几百kHz, 各阶近场信号的振幅及相位由锁相放大器直接输出至控制器拼合成图像, 每个像素点的采集时间一般在毫秒量级.

需要指出的是, 上述偶极模型是一个过度简化的模型, 它虽然能够帮助我们定性理解s-SNOM的工作原理, 但是一般不能用于近场实验数据的定量分析. 更精确的s-SNOM模型必须要把探针的几何特征包含在内[46], 例如Cvitkovic等人[47]考虑到探针柄的长度, 通过将探针简化为椭球建立起有限偶极模型, 该模型的计算结果能够与实验数据较好地吻合. 此外, s-SNOM还可以利用外差[47~50]及伪外差[51]等探测模式进一步抑制背景干扰.

2 s-SNOM应用研究进展

既然其成像对比度来自样品介电性质的变化, s-SNOM最直接的应用就是对非均相纳米材料表面介电常数ε的分布进行成像. 特别地, 一些均相纳米材料由于支持特定的电磁本征模式其光学近场呈现出对应的空间分布, 故而s-SNOM也能对这些本征模式成像. 材料的介电性质通常是光频率ω的函数, 表示为$\varepsilon(\omega)$, 利用s-SNOM及可调谐/宽带光源可以研究材料的光谱/时间色散特性; 有一些材料的介电性质同时还是波矢$\boldsymbol{k}$的函数[52], 表示为$\varepsilon(\omega,\boldsymbol{k})$, 鉴于通过近场成像可以直接获得波矢的大小, s-SNOM还可用于研究材料的空间色散/非局域效应.

2.1 介电性质分布成像

对应于特定的激发光波长, 不同的材料一般具有不同的介电性质, 因此s-SNOM可以用于低维纳米材料的特异性分辨. 如图3(a)所示, Cvitkovic等人[53]使用s-SNOM在中红外波段(λ=10.6 μm)对分散在硅基底上的金和聚苯乙烯纳米颗粒进行成像, 利用统计回归建立了由纳米颗粒直径和近场信号强度唯一确定颗粒材料种类的方法, 实现了亚10纳米颗粒的特异性识别. 对半导体材料进行掺杂会显著改变其电导率进而导致其介电性质的改变, 因此s-SNOM可以用于区分半导体材料的不同掺杂类型. 图3(b)是Stiegler等人[54]使用s-SNOM在中红外波段(λ=11.2 μm)对磷化铟纳米线的近场成像, 图像清晰地反映了硫掺杂导致的异质结结构. 相同物质在同一条件下有可能以不同的形态存在, 形成微观结构非均一的材料, 例如有机薄膜材料; s-SNOM正是研究这种非均一性的有力工具. 如图3(c)所示, Westermeier等人[55]通过中红外波段(λ=11 μm)的近场成像发现了并五苯纳米薄膜在亚微米尺度共存的两种晶相, 揭示了影响该薄膜载流子迁移率的微观原因. 考虑到探针与样品的相互作用不仅仅局限于样品表面, 在光学近场的作用深度范围之内利用s-SNOM有可能实现样品亚表面介电性质分布的成像. 图3(d), (e)分别是Taubner等人[56]和Krutokhvostov等人[57]在可见(λ=633 nm)及中红外(λ=11.3 μm)波段对亚表面金纳米结构的近场成像, 他们的结果表明s-SNOM的有效探测深度可达样品表面以下50 nm.

除上文提到的掺杂外, 应力、温度和光激发等外界条件也能对材料的介电性质产生影响, 因而利用s-SNOM可以实现外界条件调控下材料介电性质分布的近场成像. 例如Gigler等人[58]通过在中红外(λ=10.7 μm)波段对碳化硅晶体的近场成像间接获得了纳米压痕附近残余应力场的分布, 如图4(a)所示; Qazilbash等人[59]在同一波段对二氧化钒的一系列变温近场成像展示了Mott相变的微观过程, 如图4(b)所示. 除了对静态或缓变的材料介电性质分布进行高空间分辨率成像以外, 结合泵浦-探测技术s-SNOM可以实现高时空分辨率的近场成像, 记录材料介电性质随时间的动态变化过程. 例如Eisele等人[60]首先

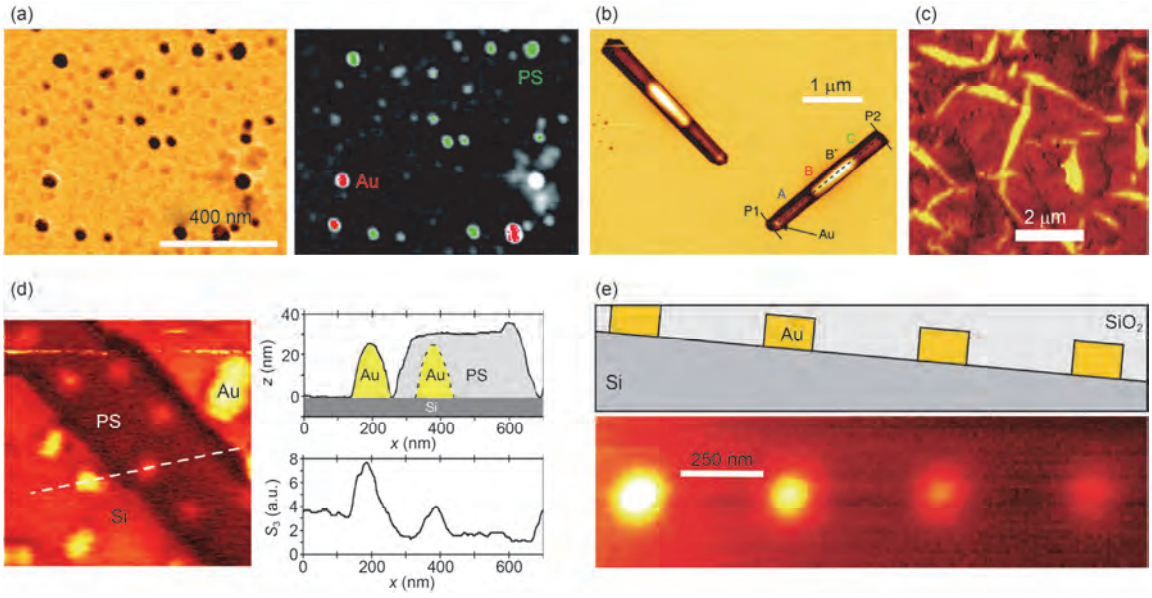

图 3 s-SNOM对非均相材料介电常数分布的成像. (a) 纳米颗粒[53]; (b) 纳米线[54]; (c) 纳米薄膜[55]; (d), (e) 亚表面金属纳米结构[56,57]

Figure 3 s-SNOM imaging of the permittivity distributions of nonhomogeneous materials. (a) Nanoparticles[53]; (b) nanowires[54]; (c) nanofilm[55]; (d), (e) subsurface metallic nanostructures[56,57]

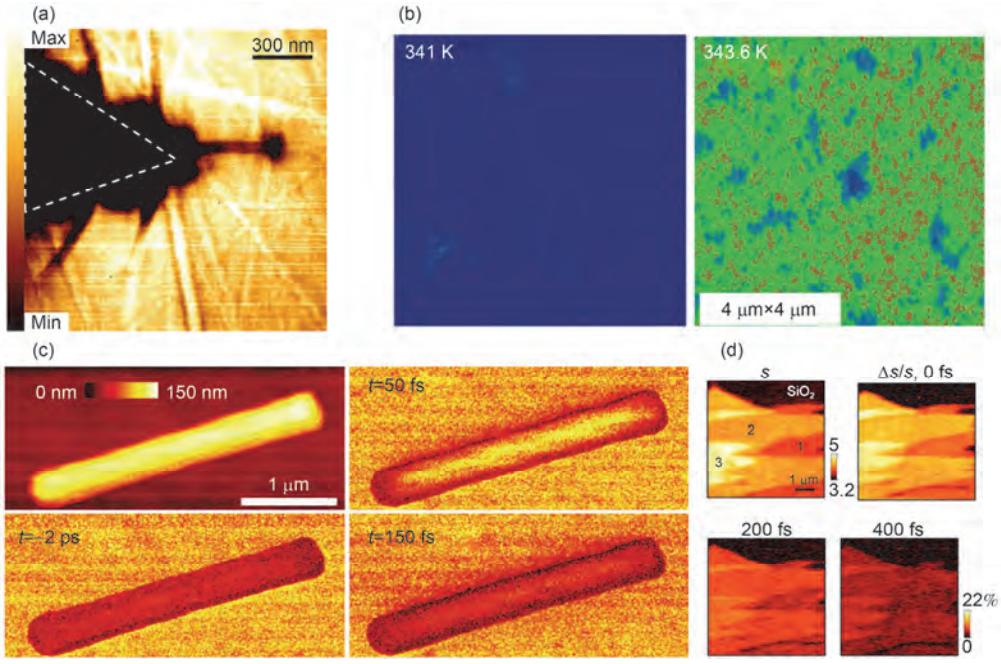

图 4 外界条件调控下低维纳米材料介电常数分布近场成像. (a) 应力[58]; (b) 温度[59]; (c), (d) 光泵浦[60,61]

Figure 4 Imaging of modulated permittivity distributions of low-dimensional materials. (a) Strain[58]; (b) temperature[59], (c); (d) light pumping[60,61]

利用近红外(λ=1.56 μm)飞秒激光脉冲泵浦砷化铟纳米线, 然后使用宽频少周期的THz脉冲对其进行近场成像, 揭示了砷化铟纳米线表面电荷的瞬态分布规律, 如图4(c)所示; Wagner等人[61]利用同样的近红外脉冲泵浦石墨烯产生热电子从而改变材料的介电性质, 然后使用中红外(λ=8.3 μm)脉冲对其进行近场成像, 最终描绘出不同层数石墨烯光生热电子的弛豫过程, 如图4(d)所示.

2.2 电磁本征模式成像

一些低维纳米材料因其几何结构和光学性质可以支持特定的电磁模式: 金属纳米颗粒及光学天线在3个空间维度对光进行约束, 可以支持非传播的电磁模式, 如局域表面等离激元[62]; 一维材料如纳米线、纳米管等在2个空间维度对光进行约束, 但允许光在其轴向传播形成导模; 二维材料仅在厚度方向对光进行约束, 允许光在其面内传播形成导模. 这些电磁模式的波矢一般远大于光在自由空间的波矢, 但s-SNOM探针可以弥补这种波矢失配进而共振激发纳米材料中的本征模式. 在共振条件下利用s-SNOM直接对纳米颗粒或光学天线进行近场成像即可得到其本征局域模式的电磁场分布; 而对一维和二维纳米材料本征导模的近场成像则需要借助材料的端点、边界等对导模的反射形成驻波来间接完成. 详细了解这些本征模式的电磁场分布对表面增强拉曼/红外基底[63,64]的优化设计及纳米波导性能的评估至关重要[65], s-SNOM正是进行电磁本征模式成像的利器.

例如Hillenbrand等人[66]利用碳纳米管修饰的探针进一步提高空间分辨率, 在可见光(λ=633 nm)波段实现了对单个金纳米颗粒电场分布的成像; Schnell等人[67]通过对红外天线(λ=9.6 μm)的近场成像系统研究了负载对天线电磁场分布的影响, 如图5(a)所示. 在一维导模成像方面, Shi等人[68]在中红外(λ=10.6 μm)波段首次观察到金属性碳纳米管可支持低损耗的拉廷格液体等离激元模式, 如图5(b)所示; 对应地, Xu等人[69]在氮化硼纳米管中发现了低损耗的声子激元模式, 如图5(c)所示; 最近, Zhou等人[70]报道了砷化铟纳米线中等离激元的观测结果. 二维材料相比一维材料种类更加繁多, 光学性质更加丰富, 同时其平面结构也更有利于扫描探针实验的开展, 因而s-SNOM在该研究领域发挥了重要作用. 例如Chen等人[71]和Fei等人[72]同时在中红外发现了电场可调谐的石墨烯等离激元模式, 如图5(d)所示; 同样在中红外, Dai等人[73]观测到了传输损耗远小于石墨烯等离激元的氮化硼声子激元模式, 如图5(e)所示; 而通过制备石墨烯-氮化硼异质结, Yang等人[74]发现利用等离激元和声子激元的相互作用可显著降低石墨烯等离激元的传输损耗. 此外, 二维材料层状结构导致的光学各向异性近来逐渐得到重视. 然而, 由于高质量范德华单晶的尺寸远小于远场光束的反射光斑, 传统的光学各向异性表征方法, 如端面反射法[75]、椭偏法[76]等, 均难以准确测量范德华微晶体的光学各向异性. 有鉴于此, Hu等人[77]提出了使用s-SNOM测量范德华微晶体光学各向异性的新方法. 图5(f)是他们在近红外(λ=1.53 μm)波段对二硫化钼导模的近场成像, 他

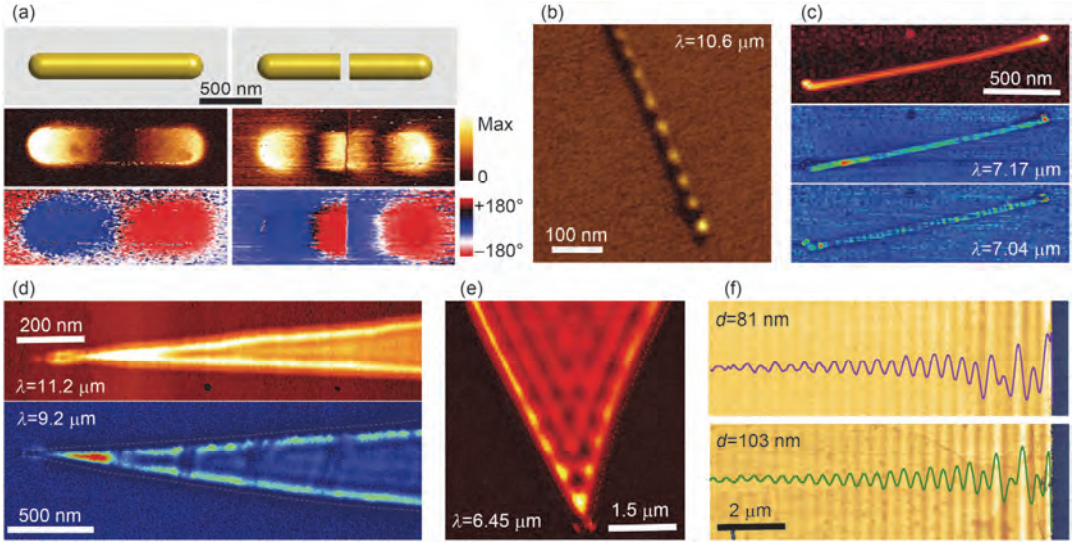

图 5 s-SNOM对低维纳米材料/结构本征电磁模式成像. (a) 红外天线[67]; (b) 碳纳米管[68]; (c) 氮化硼纳米管[69]; (d) 石墨烯[71,72]; (e) 氮化硼[73]; (f) 二硫化钼[77]

Figure 5 Imaging of the electromagnetic modes supported by low-dimensional materials. (a) Infrared antennas[67]; (b) carbon nanotube[68]; (c) boron nitride nanowires[69]; (d) graphene[71,72]; (e) hexagonal boron nitride[73]; (f) MoS_2[77]

们通过对各向异性晶体寻常及非寻常波导模式的定量分析成功地反推出了晶体的介电张量. 最近, Li等人[78]利用氮化硼制备了人工超表面并利用s-SNOM观测到了声子激元在超表面上的各向异性传播.

值得注意的是, 在上述对金属纳米颗粒或光学天线局域电磁模式进行成像的过程中往往会使用介质材料的探针, 例如硅探针. 这是因为金属探针与被测样品的相互作用较强, 探针本身既是样品局域电磁模式的激发源又是探测器, 会对被测样品的本征电磁分布产生干扰; 而使用非金属探针的s-SNOM类似于工作在收集模式的a-SNOM[79,80], 可以实现样品局域模式激发和探测的分离, 从而获得样品表面真实的电磁场分布.

还需要特别指出的是, 在上述传导型电磁模式成像实验中获得的近场图像其成像原理不尽相同. 由于一维/二维等离激元或声子激元的面内波矢远大于激发光对应的真空波矢, 这些模式在遇到材料端点或边界时以反射为主[81]; 近场图像由探针激发的入射波与来自端点或边界的反射波叠加形成, 对样品的摆放方向没有明显的依赖性; 近场图像中的干涉条纹间距等于这些模式波长的一半. 而对于二硫化钼, 其导模波矢仅稍大于激发光对应的真空波矢, 该导模在材料边界处以向远场的散射为主[77]; 近场图像由探针拾取的信号和边界散射的信号叠加而成, 对样品边界的方向具有明显的依赖性; 最终近场图像中的干涉条纹间距也包含了样品的方位信息, 这在提取导模的真实波长时必须予以消除.

将s-SNOM与超快激光技术结合可以对传播型电磁模式进行高时间分辨率的近场成像, 直接对其时间演变过程进行观测. 例如Yoxall等人[82]通过控制近场信号与参比信号的光程差直接观察到了氮化硼声子激元波包的传输过程, 如图6(a)所示, 证明了氮化硼声子激元能以极低的群速度(0.002c)传播; Huber等人[83]使用近红外脉冲(λ=1.56 μm)激发半导体材料黑磷并使用中红外脉冲(λ=8.3 μm)对其支持的等离激元进行近场成像, 研究了黑磷等离激元的光致开关特性, 测得其开启时间约为50 fs, 寿命约为5 ps. 低温环境下材料的光学性质有可能发生显著变化, 这样其支持的本征电磁模式也会随之变化, 使用s-SNOM就可以在低温条件下对这些模式进行成像研究. 图6(c)是Ni等人[84]利用自制的低温型s-SNOM在60 K对石墨烯等离激元的近场成像, 他们发现在这一温度, 电子-声子散射造成的等离激元传输损耗显著减少, 石墨烯等离激元的传输距离可达10 μm.

2.3 纳米红外光谱分析

红外光谱技术在物质种类鉴别及分析领域应用广泛, 是一种重要的材料表征手段. 但是受到衍射极限的制约, 远场红外光谱技术要求被测样品的尺寸至少要达到10 μm量级, 远大于低维纳米材料的特征尺寸. 由于s-SNOM的空间分辨率不依赖于波长, 基于s-SNOM的红外光谱技术能够突破衍射极限, 满足对低维纳米材料进行光谱分析的要求. 早期利用s-SNOM实现纳米材料红外光谱分析的实例都采用了串行扫描方法, 即利用可调谐激光器依次在多个波长对样品进行扫描成像然后将多次扫描的数据拼合成光谱[85,86]. 这种方法费时费力, 并且样品在长时间扫描过程中有可能发生位置漂移从而导致光谱测量出现误差. 后来, 随着差频红外宽带光源的出现[87], 基于s-SNOM的并行扫描红外光谱技术即得到了发展[88], 这就是纳米傅里叶变换红外光谱技术(nano-FTIR). 该技术首先利用迈克尔逊干涉仪记录被探针-样品系统散射的宽带红外光时域干涉图, 然后通过傅里叶变换反演出样品的红外吸收谱.

在使用nano-FTIR对材料进行扫描时, 每一个像素点都对应1个完整的红外光谱, 单个光谱的测量时间可缩短至10 s以下. Huth等人[89]和Amenabar等人[90]的工作都表明利用nano-FTIR得到的近场光谱与远场光谱有较好的对应性, 如图7(a), (b)所示. nano-FTIR的高空间分辨率及分子识别能力使其成为研究纳米尺度化学反应过程的有力工具, 如Wu等人[91]就利用该技术对金纳米颗粒催化的氮杂卡宾分子还原反应过程进行了研究, 如图7(c)所示. 结果表明, nano-FTIR不仅可以清晰地分辨反应过程的中间产物, 还能以纳米级的精度定位金纳米颗粒上的催化活性位点. 对于支持特定电磁本征模式的材料, 当探针远离样品边界时, nano-FTIR可用于获取该材料的红外吸收光谱; 当探针与样品边界的距离小于导模的传播距离时, nano-FTIR可用于获取该模式的频率色散特性. 图7(d)显示的是, Dai等人[73]使用nano-FTIR对氮化硼进行线扫描即可得到其声子激元波矢的频率色散特性; 由于声子激元的波矢由材料的介电性质及几何结构唯一确定, 由图7(d)便可得到氮化硼介电性质的频率色散特性.

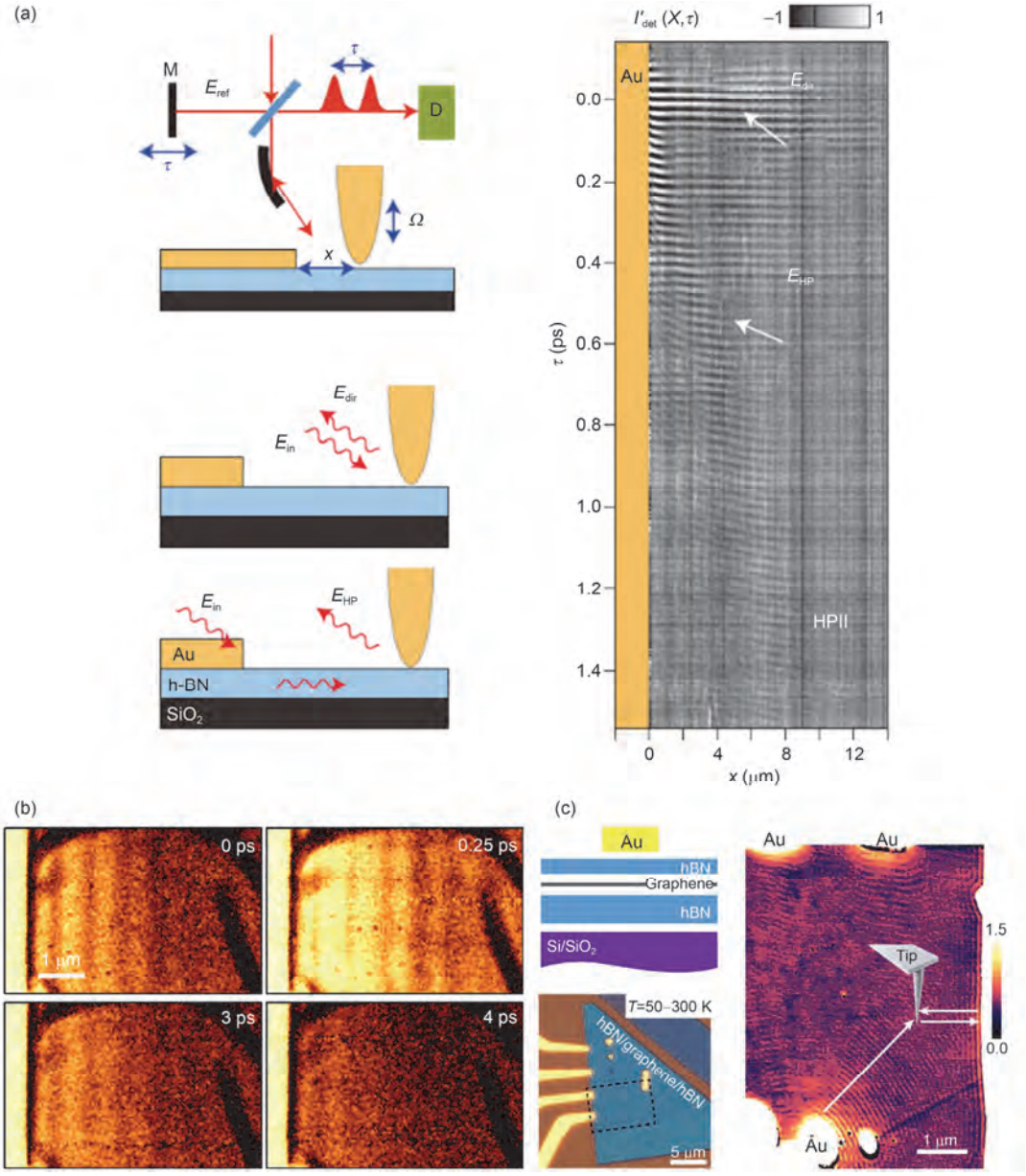

图 6 超快及低温s-SNOM对本征电磁模式的成像. (a) 氮化硼声子激元波包成像[82]; (b) 黑磷等离激元成像[83]; (c) 低温石墨烯等离激元成像[84]

Figure 6 Ultrafast and cryogenic s-SNOM imaging of electromagnetic modes. (a) Imaging of the wave packets of hexagonal boron nitride phonon polaritons[82]. (b) Imaging of black phosphorus plasmon polaritons[83]. (c) Imaging of graphene plasmon polaritons at cryogenic temperatures[84]

目前, s-SNOM的近场成像功能已经在低维纳米材料表征领域得到了广泛应用, 产出了大量相关文献, 但有关nano-FTIR的报道相对较少. 这主要是因为nano-FTIR目前采用的差频红外光源带宽较窄, 功率密度较低, 使其只能在数量有限的几个实验体系下取得高质量的光谱数据. 鉴于此, Bechtel研究组[92~94]提出利用同步辐射光源代替差频红外光源以克服其在带宽及功率密度方面的不足, 提升nano-FTIR的性能.

在上述三类应用中, 虽然s-SNOM的空间分辨率达到了10 nm量级, 但是还远大于材料中出现非局域效应所对应的尺度. 但是有些材料在特定频段会在较大空间尺度表现出非局域效应, 从而使得利用s-SNOM探测材料介电性质的空间色散成为可能. 例如石墨烯等离激元在THz频段具有很大的波矢, 致使其相速度与材料中电子的费米速度相当, 进而导致

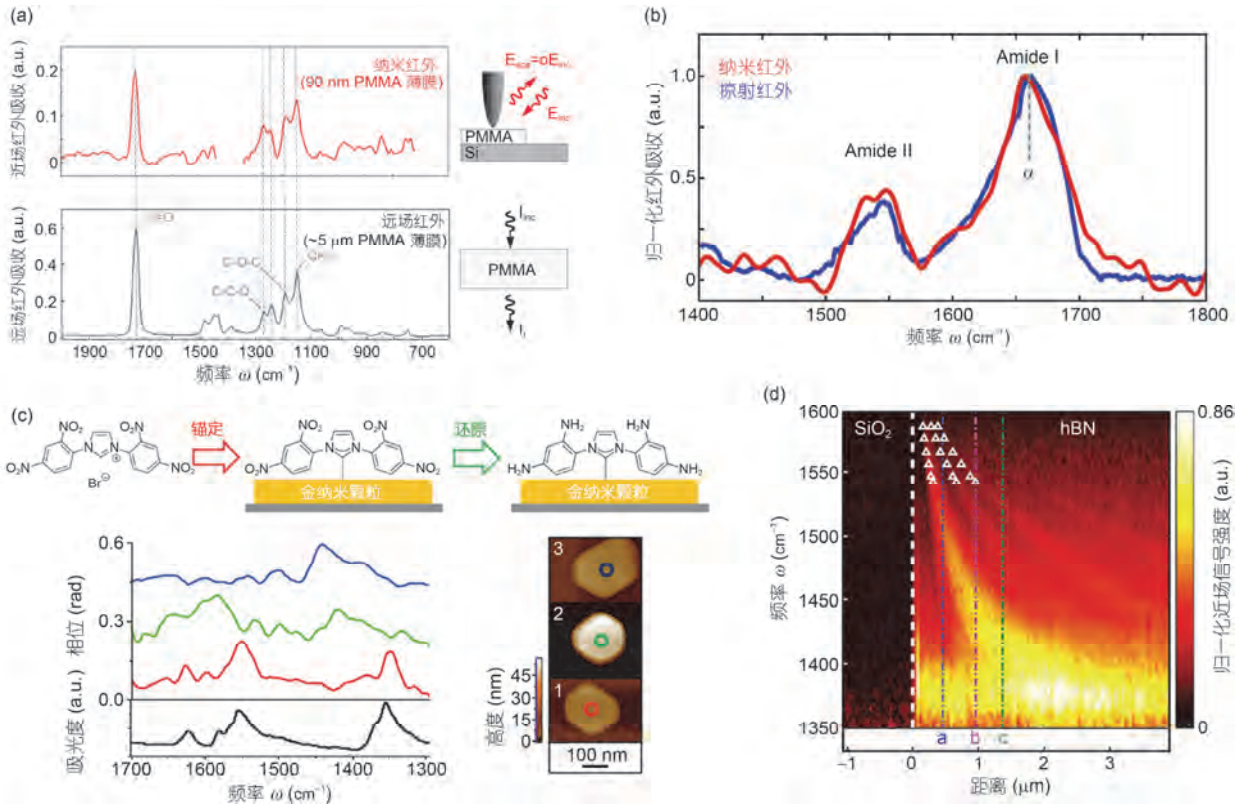

图 7 纳米红外光谱技术nano-FTIR的典型应用. (a) 聚甲基丙烯酸甲酯(PMMA)近场和远场红外光谱对比[89]; (b) 烟草花叶病毒近场和远场红外光谱对比[90]; (c) 利用nano-FTIR监测金纳米颗粒催化氮杂卡宾还原反应过程[91]; (d) 利用nano-FTIR获取氮化硼声子激元的频率色散特性[73]

Figure 7 Typical applications of nano-FTIR. (a) Comparison of the near- and far-field infrared spectra of PMMA[89]. (b) Comparison of the near- and far-field infrared spectra of tobacco mosaic virus[90]. (c) Monitoring catalytic reactions on single nanoparticles using nano-FTIR[91]. (d) Mapping dispersions of hexagonal boron nitride phonon polaritons using nano-FTIR[73]

石墨烯的光电导表现出非局域效应. Lundeberg等人[95]首先对这一效应进行了研究: 他们使用s-SNOM在THz频段(f=3.11 THz)激发石墨烯等离激元, 通过改变石墨烯的介电环境调节石墨烯等离激元的波矢大小, 利用光生电流成像来获取等离激元波矢的大小. 实验结果与理论预测十分吻合, 证明了利用s-SNOM可以对材料的时间及空间色散特性进行同步表征.

3 结语

s-SNOM突破衍射极限的高空间分辨率使其特别适合于低维纳米材料的光学表征. 借助这一技术, 国内外多个研究组针对多种低维纳米材料体系的研究都取得了出色的成果, 初步展示了s-SNOM的应用潜力. 但是要完全发挥该技术的威力, 无论是在理论模型的完善还是仪器功能的拓展方面都还有大量的工作亟待完成. 例如, 近场光学信号的定量解读目前还存在困难, 纳米红外光谱的信噪比还需提高, s-SNOM的工作频段也需要进一步拓宽. 此外, 为适应超导[96]、自旋[97]、拓扑绝缘体[98,99]等强关联材料体系的光学表征需求, 能够兼容超高真空、超低温、强磁场等极端环境的s-SNOM仪器还需要发展完善.

参考文献

1 Born M, Wolf E. Principles of Optics. Cambridge: Cambridge University Press, 1999

2 Han M, Xie B. Fundamentals of Nanostructured Materials (in Chinese). Beijing: Science Press, 2017 [韩民, 谢波. 纳米结构材料科学基础. 北京: 科学出版社, 2017]

3 Klar T A, Jakobs S, Dyba M, et al. Fluorescence microscopy with diffraction resolution barrier broken by stimulated emission. Proc Natl Acad Sci USA, 2000, 97: 8206–8210
4 Betzig E, Patterson G H, Sougrat R, et al. Imaging intracellular fluorescent proteins at nanometer resolution. Science, 2006, 313: 1642–1645
5 Rust M J, Bates M, Zhuang X. Sub-diffraction-limit imaging by stochastic optical reconstruction microscopy (STORM). Nat Methods, 2006, 3: 793–796
6 Betzig E, Trautman J K. Near-field optics: Microscopy, spectroscopy, and surface modification beyond the diffraction limit. Science, 1992, 257: 189–195
7 Hell S W. Far-field optical nanoscopy. Science, 2007, 316: 1153–1158
8 Binnig G, Rohrer H, Gerber C, et al. Surface studies by scanning tunneling microscopy. Phys Rev Lett, 1982, 49: 57–61
9 Kawata S, Ichimura T, Taguchi A, et al. Nano-Raman scattering microscopy: Resolution and enhancement. Chem Rev, 2017, 117: 4983–5001
10 Girard C, Dereux A. Near-field optics theories. Rep Prog Phys, 1996, 59: 657–699
11 Pendry J B. Negative refraction makes a perfect lens. Phys Rev Lett, 2000, 85: 3966–3969
12 Pendry J B, Smith D R. Reversing light with negative refraction. Phys Today, 2004, 57: 37–43
13 Synge E H. A suggested method for extending microscopic resolution into the ultra-microscopic region. Philos Mag, 1928, 6: 356–362
14 O'Keefe J A. Resolving power of visible light. J Opt Soc Am, 1956, 46: 359
15 Baez A V. Is resolving power independent of wavelength possible? An experiment with a sonic "macroscope". J Opt Soc Am, 1956, 46: 901
16 Wessel J. Surface-enhanced optical microscopy. J Opt Soc Am B, 1985, 2: 1538–1541
17 Reddick R C, Warmack R J, Ferrell T L. New form of scanning optical microscopy. Phys Rev B, 1989, 39: 767–770
18 Pohl D W, Denk W, Lanz M. Optical stethoscopy: Image recording with resolution *l*/20. Appl Phys Lett, 1984, 44: 651–653
19 Dürig U, Pohl D W, Rohner F. Near-field optical-scanning microscopy. J Appl Phys, 1986, 59: 3318
20 Betzig E, Isaacson M, Lewis A. Collection mode near-field scanning optical microscopy. Appl Phys Lett, 1987, 51: 2088
21 Zenhausern F, Oboyle M P, Wickramasinghe H K. Apertureless near-field optical microscope. Appl Phys Lett, 1994, 65: 1623
22 Inouye Y, Kawata S. Near-field scanning optical microscope with a metallic probe tip. Opt Lett, 1994, 19: 159
23 Zenhausern F, Martin Y, Wickramasinghe H K. Scanning interferometric apertureless microscopy: Optical imaging at 10 Å resolution. Science, 1995, 269: 1083–1085
24 Lahrech A, Bachelot R, Gleyzes P, et al. Infrared-reflection-mode near-field microscopy using an apertureless probe with a resolution of *l*/600. Opt Lett, 1996, 21: 1315–1317
25 Novotny L, Hecht B. Principles of Nano-optics. Cambridge: Cambridge University Press, 2006
26 Burresi M, van Oosten D, Kampfrath T, et al. Probing the magnetic field of light at optical frequencies. Science, 2009, 326: 550–553
27 le Feber B, Rotenberg N, Beggs D M, et al. Simultaneous measurement of nanoscale electric and magnetic optical fields. Nat Photon, 2013, 8: 43–46
28 Hecht B, Sick B, Wild U P, et al. Scanning near-field optical microscopy with aperture probes: Fundamentals and applications. J Chem Phys, 2000, 112: 7761
29 Keilmann F. Scattering-type near-field optical microscopy. J Electron Microsc, 2004, 53: 187–192
30 Taubner T, Hillenbrand R, Keilmann F. Performance of visible and mid-infrared scattering-type near-field optical microscopes. J Microsc, 2003, 210: 311–314
31 Deutsch B, Hillenbrand R, Novotny L. Near-field amplitude and phase recovery using phase-shifting interferometry. Opt Express, 2008, 16: 494–501
32 Brehm M, Frey H G, Guckenberger R, et al. Consolidating apertureless SNOM. J Korean Phys Soc, 2005, 47: S80–S85
33 Novotny L. From near-field optics to optical antennas. Phys Today, 2011, 64: 47–52
34 Novotny L, van Hulst N. Antennas for light. Nat Photon, 2011, 5: 83–90
35 Martin O J F, Girard C. Controlling and tuning strong optical field gradients at a local probe microscope tip apex. Appl Phys Lett, 1997, 70: 705
36 Knoll B, Keilmann F. Enhanced dielectric contrast in scattering-type scanning near-field optical microscopy. Opt Commun, 2000, 182: 321–328
37 Keilmann F, Hillenbrand R. Near-field microscopy by elastic light scattering from a tip. Philos Trans Royal Soc A, 2004, 362: 787–805
38 Jackson J D. Classical Electrodynamics. New York: Wiley, 1999
39 Koglin J, Fischer U C, Fuchs H. Material contrast in scanning near-field optical microscopy at 1–10 nm resolution. Phys Rev B, 1997, 55: 7977–7984
40 Raschke M B, Lienau C. Apertureless near-field optical microscopy: Tip-sample coupling in elastic light scattering. Appl Phys Lett, 2003, 83: 5089

41 Aubert S, Bruyant A, Blaize S, et al. Analysis of the interferometric effect of the background light in apertureless scanning near-field optical microscopy. J Opt Soc Am B, 2003, 20: 2117–2124
42 Bek A, Vogelgesang R, Kern K. Optical nonlinearity versus mechanical anharmonicity contrast in dynamic mode apertureless scanning near-field optical microscopy. Appl Phys Lett, 2005, 87: 163115
43 Taubner T, Keilmann F, Hillenbrand R. Effect of tip modulation on image contrast in scattering-type near-field optical microscopy. J Korean Phys Soc, 2005, 47: S213–S216
44 Hillenbrand R, Stark M, Guckenberger R. Higher-harmonics generation in tapping-mode atomic-force microscopy: Insights into the tip-sample interaction. Appl Phys Lett, 2000, 76: 3478
45 Labardi M, Patanè S, Allegrini M. Artifact-free near–field optical imaging by apertureless microscopy. Appl Phys Lett, 2000, 77: 621
46 Vogelgesang R, Kern K, Esteban R. Tip-substrate interaction in optical near-field microscopy. Phys Rev B, 2007, 75: 195410
47 Cvitkovic A, Ocelic N, Hillenbrand R. Analytical model for quantitative prediction of material contrasts in scattering-type near-field optical microscopy. Opt Express, 2007, 15: 8550–8565
48 Hillenbrand R, Keilmann F. Complex optical constants on a subwavelength scale. Phys Rev Lett, 2000, 85: 3029–3032
49 Sasaki Y, Sasaki H. Heterodyne detection for the extraction of the probe-scattering signal in scattering-type scanning near-field optical microscope. Jpn J Appl Phys, 2000, 39: L321–L323
50 Hillenbrand R, Knoll B, Keilmann F. Pure optical contrast in scattering-type scanning near-field microscopy. J Microsc, 2001, 202: 77–83
51 Ocelic N, Huber A, Hillenbrand R. Pseudoheterodyne detection for background-free near-field spectroscopy. Appl Phys Lett, 2006, 89: 101124
52 Landau L D, Lifshitz E M. Electrodynamics of Continuous Media. Beijing: Pergamon Press, 1984
53 Cvitkovic A, Ocelic N, Hillenbrand R. Material-specific infrared recognition of single sub-10 nm particles by substrate-enhanced scattering-type near-field microscopy. Nano Lett, 2007, 7: 3177–3181
54 Stiegler J M, Huber A J, Diedenhofen S L, et al. Nanoscale free-carrier profiling of individual semiconductor nanowires by infrared near-field nanoscopy. Nano Lett, 2010, 10: 1387–1392
55 Westermeier C, Cernescu A, Amarie S, et al. Sub-micron phase coexistence in small-molecule organic thin films revealed by infrared nano-imaging. Nat Commun, 2014, 5: 4101
56 Taubner T, Keilmann F, Hillenbrand R. Nanoscale-resolved subsurface imaging by scattering-type near-field optical microscopy. Opt Express, 2005, 13: 8893–8899
57 Krutokhvostov R, Govyadinov A A, Stiegler J M, et al. Enhanced resolution in subsurface near–field optical microscopy. Opt Express, 2012, 20: 593–600
58 Gigler A M, Huber A J, Bauer M, et al. Nanoscale residual stress-field mapping around nanoindents in SiC by IR s-SNOM and confocal Raman microscopy. Opt Express, 2009, 17: 22351–22357
59 Qazilbash M M, Brehm M, Chae B, et al. Mott transition in VO_2 revealed by infrared spectroscopy and nano-imaging. Science, 2007, 318: 1750
60 Eisele M, Cocker T L, Huber M A, et al. Ultrafast multi-terahertz nano-spectroscopy with sub-cycle temporal resolution. Nat Photon, 2014, 8: 841–845
61 Wagner M, Fei Z, Mcleod A S, et al. Ultrafast and nanoscale plasmonic phenomena in exfoliated graphene revealed by infrared pump-probe nanoscopy. Nano Lett, 2014, 14: 894–900
62 Wang Z L. A review on research progress in surface plasmons (in Chinese). Prog Phys, 2009, 29: 287–324 [王振林. 表面等离激元研究新进展. 物理学进展, 2009, 29: 287–324]
63 Stiles P L, Dieringer J A, Shah N C, et al. Surface-enhanced Raman spectroscopy. Annu Rev Anal Chem, 2008, 1: 601–626
64 Hu H, Yang X, Zhai F, et al. Far-field nanoscale infrared spectroscopy of vibrational fingerprints of molecules with graphene plasmons. Nat Commun, 2016, 7: 12334
65 Rotenberg N, Kuipers L. Mapping nanoscale light fields. Nat Photon, 2014, 8: 919–926
66 Hillenbrand R, Keilmann F, Hanarp P, et al. Coherent imaging of nanoscale plasmon patterns with a carbon nanotube optical probe. Appl Phys Lett, 2003, 83: 368
67 Schnell M, García-Etxarri A, Huber A J, et al. Controlling the near-field oscillations of loaded plasmonic nanoantennas. Nat Photon, 2009, 3: 287–291
68 Shi Z, Hong X, Bechtel H A, et al. Observation of a Luttinger-liquid plasmon in metallic single-walled carbon nanotubes. Nat Phys, 2015, 9: 515–519
69 Xu X G, Ghamsari B G, Jiang J, et al. One-dimensional surface phonon polaritons in boron nitride nanotubes. Nat Commun, 2014, 5: 4782
70 Zhou Y, Chen R, Wang J, et al. Tunable low loss 1D surface plasmons in inas nanowires. Adv Mater, 2018, 30: 1802551

71 Chen J, Badioli M, Alonso-Gonzalez P, et al. Optical nano-imaging of gate-tunable graphene plasmons. Nature, 2012, 487: 77–81
72 Fei Z, Rodin A S, Andreev G O, et al. Gate-tuning of graphene plasmons revealed by infrared nano-imaging. Nature, 2012, 487: 82–85
73 Dai S, Fei Z, Ma Q, et al. Tunable phonon polaritons in atomically thin van der Waals crystals of boron nitride. Science, 2014, 343: 1125–1129
74 Yang X, Zhai F, Hu H, et al. Far-field spectroscopy and near-field optical imaging of coupled plasmon-phonon polaritons in 2D van der Waals heterostructures. Adv Mater, 2016, 28: 2931–2938
75 Liang Y L. Optical anisotropy in layer compounds. J Phys C Solid State Phys, 1973, 6: 551–565
76 Weber J W, Calado V E, van de Sanden M C M. Optical constants of graphene measured by spectroscopic ellipsometry. Appl Phys Lett, 2010, 97: 91901–91904
77 Hu D, Yang X, Li C, et al. Probing optical anisotropy of nanometer-thin van der Waals microcrystals by near-field imaging. Nat Commun, 2017, 8: 1471
78 Li P, Dolado I, Alfaro-Mozaz F J, et al. Infrared hyperbolic metasurface based on nanostructured van der Waals materials. Science, 2018, 359: 892
79 Fang Z, Fan L, Lin C, et al. Plasmonic coupling of bow tie antennas with ag nanowire. Nano Lett, 2011, 11: 1676–1680
80 Fang Z, Peng Q, Song W, et al. Plasmonic focusing in symmetry broken nanocorrals. Nano Lett, 2011, 11: 893–897
81 Kang J, Wang S, Shi Z, et al. Goos-Hänchen shift and even-odd peak oscillations in edge-reflections of surface polaritons in atomically thin crystals. Nano Lett, 2017, 17: 1768–1774
82 Yoxall E, Schnell M, Nikitin A Y, et al. Direct observation of ultraslow hyperbolic polariton propagation with negative phase velocity. Nat Photon, 2015, 9: 674–678
83 Huber M A, Mooshammer F, Plankl M, et al. Femtosecond photo-switching of interface polaritons in black phosphorus heterostructures. Nat Nanotechnol, 2016, 12: 207
84 Ni G X, Mcleod A S, Sun Z, et al. Fundamental limits to graphene plasmonics. Nature, 2018, 557: 530–533
85 Stiegler J M, Abate Y, Cvitkovic A, et al. Nanoscale infrared absorption spectroscopy of individual nanoparticles enabled by scattering-type near-field microscopy. ACS Nano, 2011, 5: 6494–6499
86 Fei Z, Andreev G O, Bao W, et al. Infrared nanoscopy of dirac plasmons at the graphene-SiO_2 interface. Nano Lett, 2011, 11: 4701–4705
87 Keilmann F, Amarie S. Mid-infrared frequency comb spanning an octave based on an Er fiber laser and difference-frequency generation. J Infrared Millim Terahertz Waves, 2012, 33: 479–484
88 Amarie S, Keilmann F. Broadband-infrared assessment of phonon resonance in scattering-type near-field microscopy. Phys Rev B, 2011, 83: 045404
89 Huth F, Govyadinov A, Amarie S, et al. Nano-FTIR absorption spectroscopy of molecular fingerprints at 20 nm spatial resolution. Nano Lett, 2012, 12: 3973–3978
90 Amenabar I, Poly S, Nuansing W, et al. Structural analysis and mapping of individual protein complexes by infrared nanospectroscopy. Nat Commun, 2013, 4: 2890
91 Wu C, Wolf W J, Levartovsky Y, et al. High-spatial-resolution mapping of catalytic reactions on single particles. Nature, 2017, 541: 511
92 Bechtel H A, Muller E A, Olmon R L, et al. Ultrabroadband infrared nanospectroscopic imaging. Proc Natl Acad Sci USA, 2014, 111: 7191–7196
93 Hermann P, Hoehl A, Ulrich G, et al. Characterization of semiconductor materials using synchrotron radiation-based near-field infrared microscopy and nano-FTIR spectroscopy. Opt Express, 2014, 22: 17948–17958
94 Patoka P, Ulrich G, Nguyen A E, et al. Nanoscale plasmonic phenomena in CVD-grown MoS_2 monolayer revealed by ultra-broadband synchrotron radiation based nano-FTIR spectroscopy and near-field microscopy. Opt Express, 2016, 24: 1154–1164
95 Lundeberg M B, Gao Y, Asgari R, et al. Tuning quantum nonlocal effects in graphene plasmonics. Science, 2017, 357: 6347
96 Cao Y, Fatemi V, Fang S, et al. Unconventional superconductivity in magic-angle graphene superlattices. Nature, 2018, 556: 43
97 Žutić, I, Fabian J, Das Sarma S. Spintronics: Fundamentals and applications. Rev Mod Phys, 2004, 76: 323–410
98 He K, Wang Y Y, Xue Q K. Topological insulator and the quantum anomalous Hall effect (in Chinese). Chin Sci Bull (Chin Ver), 2014, 59: 3431–3441 [何珂, 王亚愚, 薛其坤. 拓扑绝缘体与量子反常霍尔效应. 科学通报, 2014, 59: 3431–3441]
99 Zhang S, Qi X. Topological insulators and superconductors. Rev Mod Phys, 2011, 83: 1057–1110

Summary for “低维纳米材料的近场光学表征”

Near-field optical characterization of low-dimensional nanomaterials

Debo Hu & Qing Dai*

Division of Nanophotonics, National Center for Nanoscience and Technology, Beijing 100190, China
* Corresponding author, E-mail: daiq@nanoctr.cn

Due to the wave nature of light, the spatial resolution of traditional far-field optical microscopy is fundamentally prohibited to be much smaller than the wavelength, thus cannot fulfill the requirement of nano-characterization of low-dimensional materials. This diffraction limit can be circumvented by the optical version of scanning probe microscopy via incorporating the near-field optical information into the imaging process. In the last one and a half decades, scanning near-field optical microscopic techniques, especially scattering-type scanning near-field optical microscopy (s-SNOM), have undergone tremendous development. The wavelength independent spatial resolution of s-SNOM goes far beyond the diffraction limit, leading to an explosive amount of applications that spread throughout the field of materials science.

The instrument of s-SNOM is a delicate combination of optical and scanning probe techniques. It utilizes the sharp tip of an atomic force microscope (AFM) probe to achieve nanoscale spatial resolution. Specifically, the light beam from a source is focused onto the apex of the AFM tip by a parabolic mirror. The tip serves as a nanoscale light confiner and enhancer, inducing a strong electromagnetic field (hot spot) underneath the tip apex. When the tip is brought into contact with the investigated sample, this field is modified by its interaction with the sample and carries near-field information of the sample. Then the tip acting as an optical antenna scatters the near-field information into far-field. The back-scattered near-field signals are feed into a photodetector to register a near-field image of the sample. By modulating the near-field signal via tapping the AFM tip and demodulating at the high order harmonics of the tip-tapping frequency, the noise from the background and stray light can be greatly suppressed. Since the near-field hot spot is on the same scale with the tip apex, the spatial resolution of s-SNOM is predominantly defined by the dimensions of the tip; a value of 20 nm is routinely achievable with commercially available and economical AFM tips.

In principle, s-SNOM is a permittivity-sensitive technique, thus its most typical application is to imaging the surface permittivity distributions of low-dimensional nanomaterials. In the literatures, s-SNOM has been used to realize material-specific identification of zero-dimensional nanoparticles; nanoscale-resolved mapping of the free-carrier distribution along a one-dimensional nanowire and two-dimensional nanoimaging of the phase boundaries of organic thin films have been reported. Surprisingly, sub-surface imaging of objects with a depth of tens of nanometers has also been proved possible. By using the pump-probe method, the ultrafast dynamical properties of low-dimensional materials can be characterized with simultaneously high spatial and temporal resolutions.

The s-SNOM tip can also serve as a momentum matcher between the free-space light and the intrinsic electromagnetic modes supported by low-dimensional materials, therefore, s-SNOM can be used to excite and image these modes. Both field mapping of localized modes in zero-dimensional materials and fringe pattern imaging of propagating modes in one- and two-dimensional materials have been reported. What is more, direct imaging of the wave packets has also been achieved by coupling s-SNOM to ultrafast optics.

s-SNOM can provide spectral information of the sample if a broadband light source is used. A Fourier transform infrared (FTIR) spectrometer based on s-SNOM (nano-FTIR) has been developed. The spectra obtained by nano-FTIR have been demonstrated to be in good agreement with those acquired by conventional FTIR. Applications of the nano-FTIR including *in-situ* monitoring of chemical reactions and quick mapping of the dispersion of polaritons have been reported.

In summary, s-SNOM has contributed significantly to the field of low-dimensional material characterizing. Nonetheless, it still has a large potential to expand its scope of applications. This is especially true at extreme conditions like ultrahigh vacuum, ultralow temperature, and strong magnetic field. If s-SNOM operating in these extreme conditions can be developed, it would be of great help in solving the enigma of strongly correlated materials.

diffraction limit, low-dimensional materials, near-field optical imaging, electromagnetic modes, nano-infrared spectroscopy

doi: 10.1360/N972018-00864